High Voltage Hybrid Generator and Conversion System for Wind Turbine Applications

Omid Beik, *Member, IEEE*, Nigel Schofield *Member, IEEE*

***Abstract*—This paper presents the design of a high voltage hybrid generator (HG) and conversion system for wind turbine applications. The HG combines wound field (WF) and permanent magnet (PM) rotor excitations. At any given speed, the PM induces a fixed stator voltage while the WF induces a variable controlled stator voltage. The HG alternating output is rectified via a passive rectification stage, hence the machine net DC output voltage is controlled over a prescribed, but limited range. The split ratio between PM and WF rotor sections is considered as varying from a fully WF rotor, or traditional synchronous generator (SG), to some ratio of PM to WF excitation. The turbine operational characteristics and maximum wind velocity variations between turbines in a wind farm are used to define the WF to PM split ratio. Both a 3-phase and a 9-phase stator winding design are investigated. The 9-phase winding results in 4.2% higher output RMS voltage that yields a more power dense solution. It further yields lower rectified DC-link voltage ripple. The HG mass, loss audits and efficiency discussions are presented. In order to investigate the feasibility of the HG concept a small scale laboratory prototype is designed and operational test results presented that show good agreement with the simulation model results.**

***Index Terms*—Hybrid generator, HVDC, wind energy conversion, wind turbine.**

I. Introduction

DIFFERENT turbine-generator topologies, both direct drive and geared, have been proposed in literature and developed by manufacturers. Doubly-fed induction generators (DFIG) with three-phase stator and wound rotor windings connected to the grid using two back-to-back voltage source converters (VSCs) are discussed in [1]-[2]. A typical DFIG speed range is around ±30% of its synchronous speed and since only a portion of the generated active power flows through the rotor, the VSCs power ratings are around 30% of the generator rating [3]. For a wider speed range, turbine-driven induction generators (IG), permanent magnet (PM) generators and wound field synchronous generators (SG) are connected to the grid via two full-rated VSCs in a back-to-back configuration. The two VSCs decouple the generator from the fixed frequency and voltage constraints of the AC power grid, thus allowing variable speed operation of the wind turbine. The generator-side VSC controls the machine speed via vector control to extract maximum wind power while the grid-side VSC performs active and reactive power control and maintains a near fixed intermediate DC-link voltage.

The IG is a mature technology, relatively inexpensive, robust and requires low maintenance [4]. A comparison in terms of hardware components, operation and energy output between DFIG and IG is presented in [5]. PM machines have higher flux-densities and lower losses compared to IGs and DFIG and are thus usually more power-dense. Further, being brushless, they do not need external rotor supply via slip-rings unlike DFIGs [4]. Hybrid excitation generator topologies have previously been proposed for wind turbine applications [6]-[7]. The hybrid excitation PM generator proposed by [6] has a DC wound field winding in the stator to regulate the machine output voltage while the hybrid topology proposed in [7] has two stators and an outer rotor with 24 salient poles which have no windings. The outer stator has a 3-phase winding while the inner stator uses both PM and DC wound field windings. The hybrid machine configurations in [6]-[7] are magnetically complex, low voltage (max. 220 V) and low power (up to 2 kW), and are hence of little merit in comparison to the machine design discussed in this paper. A comparison between large scale geared and direct-drive generators for wind turbine applications is presented in [8]-[10]. The comparison in [10] is based on the machine mass, energy yield, losses and cost, but neglecting the gearbox impact on these assessment criteria. An overview of wind turbine systems in terms of generator technology, power electronic interface and control strategies is provided in [11] with discussions on system issues including harmonics and faults. However, comparisons in [8]-[11] do not include a total wind generation scheme; hence they are not comprehensive and cannot be generalized. Most turbine generator systems are rated to an upper voltage limit of 1000 VAC. Although there are a few development and experimental systems using higher voltage generators, such as a geared SG operating at 13.8 kV [12] and geared PMG rated at 3.3 kV [13]. This paper proposes a high voltage hybrid generator (HG) design for

Manuscript received January 06, 2017; revised April 06, 2017; accepted August 10, 2017.

Omid Beik is with Magna Powertrain Inc., Toronto, Ontario, Canada. (e-mail: omid.beik@ieee.org).

Nigel Schofield is with the School of Computing and Engineering, University of Huddersfield, UK. (e-mail: n.schofield@hud.ac.uk).

wind turbine applications. The HG combines wound field (WF) and permanent magnet (PM) excitations on a single machine rotor. This paper also presents detailed discussions on choice of split ratio between PM and WF rotors. A 9-phase stator winding is considered for the HG, a choice that results in improved machine power density above 3-phase implementations. Moreover, the multiphase design improves the machine rectified output power quality, thus reducing the mass and volume of passive smoothing capacitors. Note that DC-link stabilization and fault ride through are out of the scope of this paper and hence not considered here.

II. Hybrid Generator (HG) Concept and Turbine Operational Characteristics

In general, PM machines have a fixed rotor field excitation that induces a fixed voltage in the stator winding at a fixed speed. Therefore, in order to control the machine a full-rated power electronic converter is required. However, if the converter is eliminated an alternative solution is required to regulate machine output voltage or current, and hence power. The HG proposed in this paper is an AC machine having a 9-phase, high voltage (6.87 kV RMS phase at 600 RPM) stator winding and utilizing two rotor sections, namely a PM rotor and a WF rotor. The name hybrid generator refers to the combination of these two rotors excitations. A schematic view of the HG is depicted in Fig. 1(a). The PM and WF rotor sections exist on one rotor assembly inside one machine housing. Therefore, the HG combines the output voltage due to a fixed field from the PM rotor and a controlled variable voltage due to the variable field of the WF rotor. The total machine output voltage is the sum of the voltages due to the PM and WF sections. The range of the total voltage variation depends on the range of the WF excitation to that of the PM field excitation, referred to here as the field excitation split ratio for the HG. DC current for the WF rotor excitation is provided via a brushless exciter system common to industrial synchronous machine systems. The brushless exciter has an AC rotor winding that may use a 3-phase or multiphase configuration. Output of the brushless exciter rotor is then connected to a rotating rectifier that in turn provides the DC supply to the HG WF. A multiphase design for the brushless exciter gives good DC output quality (lower voltage ripple) and higher output voltage when compared to those of a conventional 3-phase exciter. The HG configuration with a passive rectifier for a wind turbine application is shown schematically in Fig. 1(b). The brushless exciter has a DC stator winding that is fed via controlled rectified output of the HG. The HG has been proposed for an off-shore wind generation scheme with high voltage DC transmission and interconnection system, as discussed by the authors in [14]. The study in [14] was a conceptual feasibility study to assess the relative merits of an HVDC HG system against existing industrial practice. In this paper, two European wind farms are chosen as application references for the HG since the machine output specification closely fits the voltage levels within the farms. Further, the machine design developed in this paper utilizes standard machine insulation systems and design procedures, and thus illustrates a solution that could immediately compete in current wind farms. The reference wind farms chosen are the Trianel (TR) and Borkum Riffgrund (BR) wind farms connected to the DolWin 1 HVDC off-shore converter station in the southern part of the German Bight [15], Fig. 2(a). There are 78 Siemens geared IG rated at 4 MW, 690 V in the BR wind farm while the TR wind farm has 80 AREVA PM generators rated at 5 MW, 3.3 kV. In both the TR and BR farms each generator output is electrically connected via two back-to-back VSCs and a tower mounted step-up transformer to 33 kVAC. The outputs from multiple turbines, 78 and 80 respectively, are combined and stepped-up to 155 kV for transmission over a distance of 7.5 km to the DolWin 1 off-shore converter station where it is brought to the desired HVDC level of ±320 kV via two parallel 590 MVA transformers and rectification equipment before transmission to shore via HVDC cables, Fig. 2(a).

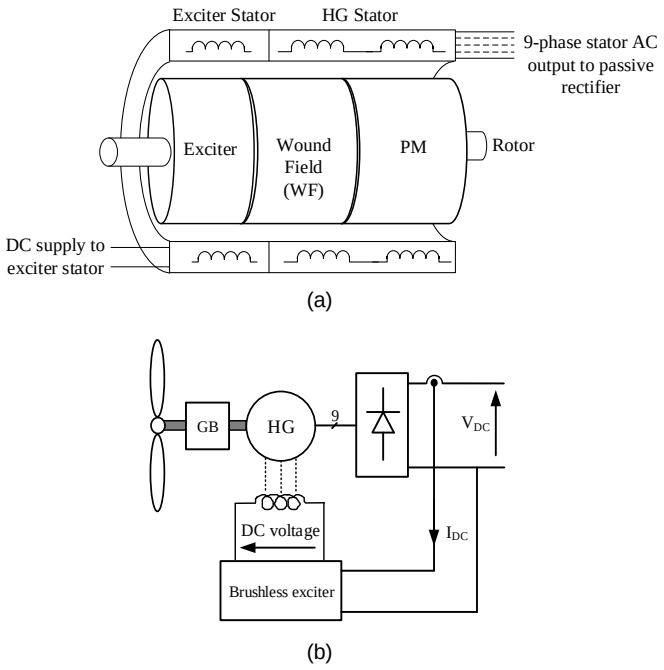

Fig. 1. Hybrid generator (HG) concept. (a) Schematic. (b) Wind turbine application.

It is proposed here that the HG design would replace the IG and PM generators in the TR and BR wind farms, as shown in Fig. 2(b). The two VSCs are replaced with a passive rectifier, the tower transformer is eliminated and the turbine DC output is sent to the off-shore substation where is it converted back to AC and sent to the HVDC converter station. The DC/AC conversion at the off-shore substation in Fig. 2(b) includes (i) DC/DC conversion to provide a fixed DC voltage (V_dc2) and ensure operation of the system and, (ii) an inverter stage to interface the system to the fixed voltage and frequency grid. Note that each isolated DC/DC converter stage combines the output of a group of turbines and provides galvanic isolation using medium-to-high frequency transformers.

The HG scheme therefore reduces turbine plant and hence system mass while accessibility and maintenance is improved [14], [16]. The interconnection cable voltage for the existing systems is 33 kVAC, while it is 38.1 kVDC for the proposed

system which results in equitable interconnection cable mass given the same copper loss, current density and hence similar thermal performance for the AC and DC interconnection cable systems. The proposed HG rated output power is 5 MW at a nominal speed of 600 RPM. Designs are presented for 3-phase as well as 9-phase stator windings with a rated phase voltage of 6.87 kV. Note, phase voltage is quoted here for the HG since there are four different line-to-line voltages specified for a 9-phase system. The 3-phase stator winding is double layer while the 9-phase is four-layer comprising of two independent, double layer, 9-phase, star connected windings, the outputs of which are connected to a passive full-bridge rectifier. The two rectifier outputs are series connected to produce a combined maximum 38.1 kV DC-link voltage.

The output power of the wind turbine varies with wind velocity however turbines are generally designed and controlled to deliver a rated power over a range of wind velocity variations. Fig. 3(a) shows the published output

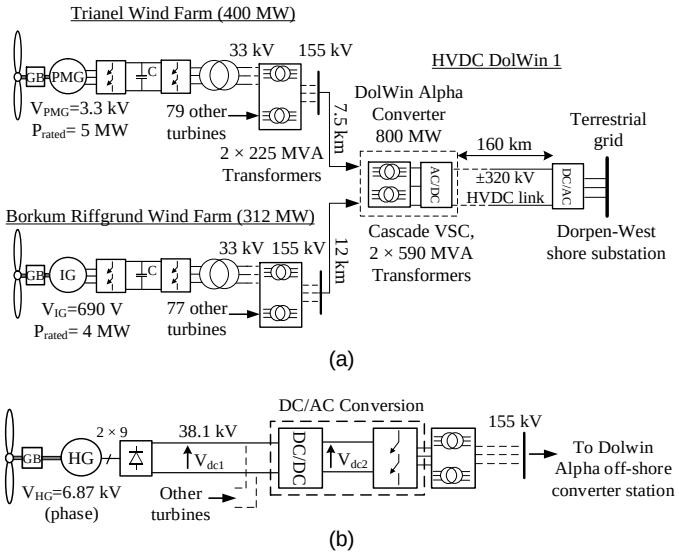

Fig. 2. (a) Trianel and Borkum Riffgrund wind farms connection to DolWin 1 HVDC off-shore converter station. (b) Proposed HG in existing system.

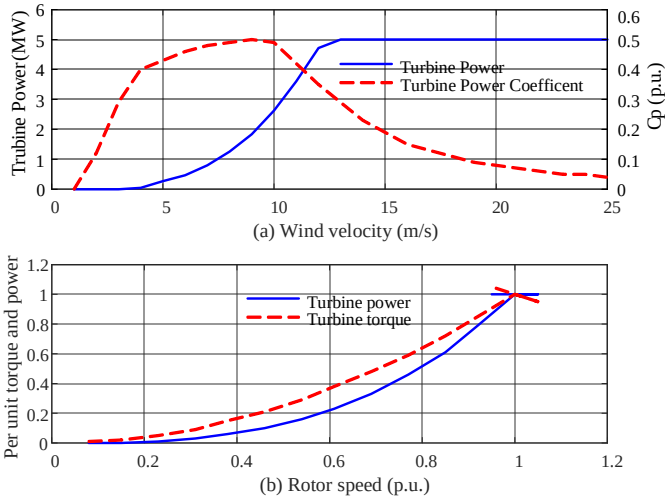

Fig. 3. AREVA Wind M5000 [13]. (a) Turbine power with wind velocity variations. (b) Turbine power- and torque-speed characteristics.

power and power coefficient of the AREVA Wind M5000 with respect to wind velocity variation [13]. Using the turbine operational data and power coefficient, the power-speed and torque-speed characteristics are calculated and presented in Fig. 3(b) assuming the wind turbine operates on a maximum power point tracking (MPPT) curve. As wind velocity varies from cut-in (4m/s) to rated velocity (12.5m/s) the generator rotor speed, power and torque increase. However, above rated wind velocity and below cut-out velocity the turbine is controlled to operate at and around a base rotor speed while delivering a rated power as shown in Fig. 3(b). It might be practically infeasible to control the turbine to operate at exactly the generator rated rotor speed and a limited speed variation is allowed (e.g. 10% around the rated speed).

The induction and PM generators in the reference system, Fig. 2(a), operate at variable speed and hence voltage, however the remaining electrical system is required to be operated at an essentially constant (nominal) voltage at all times and for all wind speed conditions. This is to ensure operation of the back-to-back VSC's and ancillary components. However, for the proposed HV scheme two control methods could be considered for the HG output DC-link voltage, (i) fixed voltage and (ii) variable (but controlled) voltage. In the fixed voltage approach the rectified output voltage of the HG in Fig. 2(b) (V_{dc1}) is maintained around its nominal DC value at all wind speed conditions i.e. from cut-in to cut-out velocities. This is implemented by controlling the WF current. In this case the voltage transfer ratio of the DC/DC converters at the off-shore substation in Fig. 2(b) is fixed. There will be small differences in voltage transfer ratios amongst the DC/DC converters to maintain power flow and avoid rectifier turn-off due to small variations in the individual turbine velocities or turbine local wind velocity. Such a control philosophy wound necessitate a high wound field variation that would result in an excessive overdesign of the HG.

In the second control scheme the rectified output voltage of the HG system (V_{dc1}) varies with wind velocity below the rated velocity. Above the rated velocity the WF is controlled to maintain the DC-link at nominal maximum. As before, there will be small perturbations in voltage for each generator around the system nominal operating value due to turbine and localized wind transients. Therefore, the voltage of the interconnection cables between the wind turbines and the off-shore substation (V_{dc1}) are allowed to vary with wind speed, but controlled between the connecting turbines via their respective HG wound field to ensure power flow. The off-shore DC/DC converter output voltage (V_{dc2}) is controlled to be fixed to ensure operation of the inverter stage and the connecting systems to shore. Consequently, the off-shore DC/DC converters have a variable voltage transfer ratio achieved by choice of the DC/DC isolation transformer turns ratio and/or by a 2- or multi-stage DC/DC converter topology.

For this study, the variable voltage control scenario with variable voltage transfer ratio DC/DC converter at the off-shore substation is chosen since this configuration results in a lower WF current requirement and hence machine mass for the HG and ensures that the off-shore to on-shore cables operate at full voltage, thus minimizing Ohmic loss.

This article has been accepted for publication in a future issue of this journal, but has not been fully edited. Content may change prior to final publication. Citation information: DOI 10.1109/TIE.2017.2748054, IEEE Transactions on Industrial Electronics

III. HG Design Consideration

A. HG Structure

As discussed, the HG rotor is comprised of WF and PM rotor sections. Fig. 4 shows cross-sectional views of the HG stator and rotors. The HG shares a common stator between WF and PM rotors. The WF rotor has 10 salient poles whose "shoe" length varies from the middle of the pole to the corners. Therefore, the WF section does not have a constant air-gap over the pole-face, referred to here as 'adjusted' air-gap a feature that reduces cogging torque compared to a constant air-gap machine. The PM material used is Sintered Neodymium-Iron-Boron (NdFeB), a rare-earth magnet material that has been used in wind applications due to its high energy density [17]-[18]. The PM rotor poles are full-pitched and mounted on the rotor surface, i.e. a cylindrical rotor as opposed to the salient WF rotor. Due to the circumferentially long magnet length (670 mm), each magnet is split into 6 equal sections with each section magnetized separately on a fixed axis relative to the magnet piece center-line. This will prevent the magnet being magnetized unevenly which would result in lower flux-density in some locations in the magnet. Table I summarizes main HG dimensions.

The HG stator has 135 slots giving 4.5 and 1.5 slots per pole per phase for 3- and 9-phase windings respectively, hence facilitating a short-pitched, fractional-slot distributed winding with a 12 slots coil span. For the same ampere-turn and total copper loss the number of turns in the 9-phase winding is 3 times that of the 3-phase [16], [19]. Therefore, for the same output power the 9-phase phase current is one third of the 3-phase phase current and keeping the same total copper area the turn cross-sectional area in the 9-phase winding is one third that of the turn cross-sectional area in the 3-phase winding. The cross-section of a stator slot including cross-section of coils is shown in Fig. 5. The coils in the slot are separated using insulating material to withstand a maximum line-to-line voltage. The HG WF DC rotor winding consists of 10 coils of 51 turns, each coil wound around one salient pole.

TABLE I
HG Dimensions

Parameter	Value
Stator outer diameter (mm)	2700
Stator inner diameter (mm)	2150
Number of stator slots	135
Stator tooth tip width (mm)	31.35
Stator slot width (mm)	18.50
Stator slot length from air-gap (mm)	90
Stator slot length for winding (mm)	87
Wedge length (mm)	5
Stator back-iron thickness (mm)	180
Stator slot area available for winding (mm^2)	1609.5
Shaft diameter (mm)	400
Bearing diameter (mm)	250
Bearing length (mm)	200
WF section minimum air-gap length (mm)	7
WF section maximum air-gap length (mm)	11
WF maximum rotor diameter of body (mm)	2136
Rotor pole body height (mm)	195
Rotor pole body width (mm)	350
Rotor pole shoe minimum height (mm)	43.7
PM thickness (mm)	40

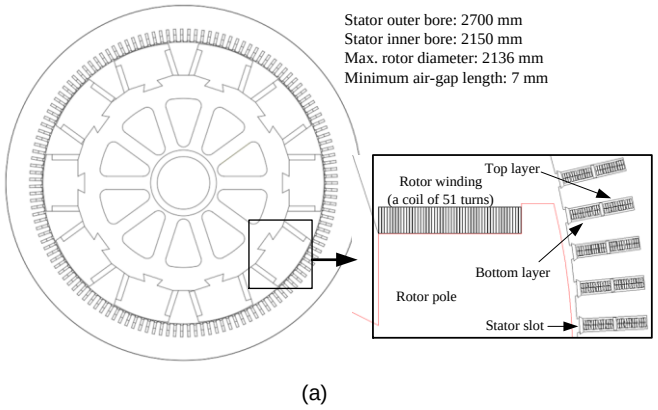

Fig. 4. HG structure. (a) Machine cross-section viewed from WF side. (b) Machine cross-section viewed from PM side. (c) WF pole details.

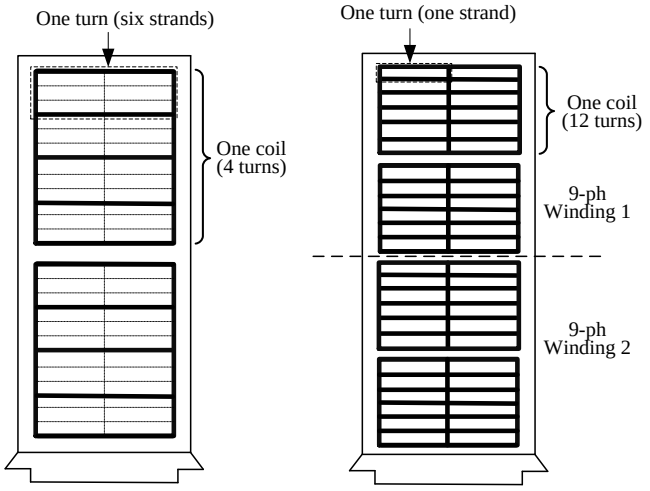

Fig. 5. Stator slot cross-section. (a) 3-phase winding. (b) 9-phase winding.

B. WF and PM Split Ratio

In a wind farm the wind turbines experience varying wind velocity with time. This is due to uneven distribution of the wind mass, uncertainty of the wind direction and also the location of the wind turbines. Therefore, in a large farm the output voltage and power of the wind turbine generators will vary slightly from one to another [20-22].

This article has been accepted for publication in a future issue of this journal, but has not been fully edited. Content may change prior to final publication. Citation information: DOI 10.1109/TIE.2017.2748054, IEEE Transactions on Industrial Electronics

For systems typical of the Trianel and Borkum Riffgrund wind farms, Fig. 2(a), the two back-to-back VSCs decouple the generator variable output voltage and frequency from the fixed voltage and frequency of the grid. However, in the proposed HG system there are no VSCs, instead the HG is connected to a passive rectifier, Fig. 1, that has no control functionality. Therefore, the WF of the HG must provide the generator output voltage control. Since the rectified outputs from all the HG's in the wind farm are electrically connected in parallel, any voltage disparity between generators will cause the rectification stage to turn off. Therefore, the WF must be designed to cater for the largest wind velocity variation between the wind turbines in the wind farm. A maximum of 18% wind velocity variation between individual wind farm turbines at any given time is reported in the literature [20-22]. Hence, in this paper, a maximum wind velocity variation of 25% is considered for the HG design to provide some design margin. The split between PM and WF rotor sections can be considered as varying from a fully WF rotor (or traditional SG rotor), to some ratio of PM to WF excitation, herein referred to as the rotor slit ratio. To satisfy the 25% wind velocity variation a HG with a PM/WF split ratio of 3:1 (i.e. 0.75/0.25) is considered and compared with a 1.0 p.u. (100%) WF design, or SG. Fig. 6 presents the total terminal voltage of a SG and HG versus rotor speed while the wind turbine is operating from cut-in to cut-out wind velocity. The machine terminal voltage is considered to be proportional to the rotor speed since the rotor WF current is fixed. There are some speed perturbations around the rotor base speed which explains the voltage perturbations around 1.0 per-unit base speed. The speed variation around rated speed is about 10%, arising from the result of practical implementation of the rotor blade pitch angle control [23]. At each rotor speed the voltage due to the PM rotor is constant while the voltage due to the WF rotor is controlled by the WF current. Using the WF back-EMF coefficient (Vs/rad) obtained from finite element analysis (FEA), the required axial length for a fully WF generator (SG) with 1.0 p.u. terminal voltage is calculated and referred to here as 1.0 p.u. axial length. Similarly, using the PM and WF back-EMF coefficients, for a HG with 1.0 p.u. terminal voltage the axial length is calculated as 0.81 p.u. comprising of 0.56 p.u. PM axial length and 0.25 p.u. WF axial length, all relative to the 1.0 p.u. SG. The field current in the SG is maintained at 1.0 p.u. while the HG WF current is scaled based on the ratio of the HG WF axial length to that of the SG. Maintaining a fixed field current throughout the wind velocity variations results in an efficient and cost effective use of the copper and wound field material. Fig. 7 illustrates the HG output voltage and torque angle characteristics at full-load with full WF current. The machine terminal voltage is derived from the per-phase flux-linkage obtained via FEA. By maintaining a rated stator current distribution and rotating the rotor, the machine static electromagnetic torque versus rotor angle is calculated via FEA and plotted in Fig. 7(b). The ratio of 9- to 3-phase RMS voltages is 1.0417, yielding an increased voltage for the 9-phase case due to an improved winding factor. Therefore, compared to the 3-phase stator winding, the 9-phase winding results in 4.2% higher output voltage at the machine terminals, resulting in a 4.2% increase in output power/torque and hence a more power dense machine. Note that the angular difference (phase shift) between the two windings is simply due to a shift in the coil center reference. Further, since the machine is connected to a passive rectifier in the proposed wind generation scheme, Fig. 1(b), it is no longer necessary to have a sinusoidal output voltage; indeed a move towards a more trapezoidal waveform yields a reduced DC-link voltage ripple.

The cogging torque for constant and adjusted air-gap rotor topologies is plotted in Fig. 7(c). The HG peak cogging torques calculated at no-load for the constant and adjusted air-gap rotor topologies are 1.86 kNm and 0.08 kNm respectively. Therefore, the adjusted air-gap results in a 95.7% reduction in cogging torque. The machine torque versus rotor angle at full-load stator phase current (peak 170.67 A) and full-field field current (486.23 A) is presented in Fig. 7(b). The HG total torque consists of torque produced by WF and PM sections.

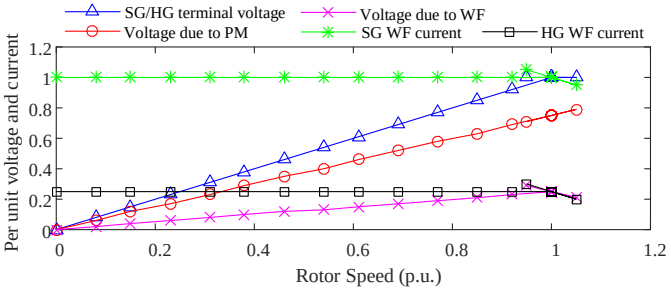

Fig. 6. Fully wound field rotor (SG) and HG voltage and current.

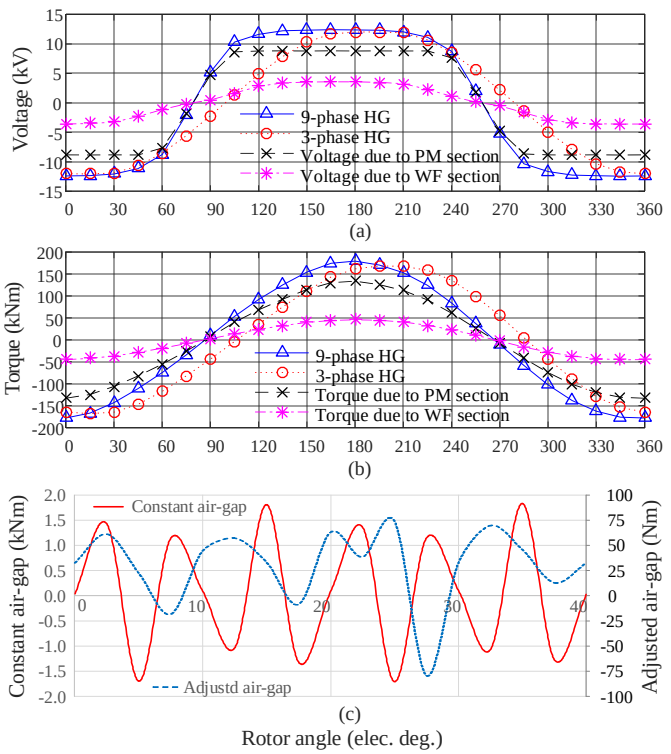

Fig. 7. Comparison of 3- and 9-phase HG. (a) Back-EMF. (b) Air-gap torque. (c) Cogging torque.

The surface PM section is magnetically a cylindrical rotor contributing only to the excitation torque. The WF has a salient rotor with two torque components, an excitation torque and a salient torque. However, the results are not as would be expected from contemporary machines theory. This feature was investigated further by varying the stator current amplitude, and then the rotor field current amplitude. There is near linear variation of peak torque with respect to stator load current. However, as the rotor field current decreases the machine magnetics move from saturation and the salient torque becomes more apparent in the machine total torque versus angle characteristics. Thus, at full rotor field current, saturation in the WF rotor (and to some extent the stator) results in a lower saliency ratio and hence salient torque contribution leaving the excitation torque the dominant component. Note that although the PM and WF sections share the same stator they operate at different flux densities.

The air-gap flux-density for the WF section is 0.998T at full-field excitation while it is 0.85T for the PM section to avoid stator saturation. Some parts of the stator back-iron, tooth and rotor laminations for the WF section operate at flux densities close to 2T and are hence saturated facilitating reduced inductance and hence better power capability. The HG inductance consist of two components, (i) inductance due to WF section that changes with rotor angle due to rotor saliency, and (ii) PM section inductance that is constant. Fig. 8(a) shows nine coils each representing one phase where the displacement between adjacent coils is 40 electrical degrees. Equation (1) is adopted to model the self- and mutual-inductances for the 9-phase winding:

$$\begin{aligned} L_i &= L_0^{PM} + L_0^{WF} + L_g^{WF}\cos(2\theta_e+\beta), \qquad i=1,\ ...,9 \\ M_{1i} &= \left(L_0^{PM}+L_0^{WF}\right)\cos(\beta)+L_g^{WF}\cos(2\theta_e-\beta),\ i=2,...,9 \\ \beta &= (2i-2)\frac{\pi}{9} \end{aligned} \tag{1}$$

where, i is phase number, L_i is phase self-inductance, M_{1i} is the mutual inductance between phase 1 and phase i, L_0^{PM} is the PM section self-inductance, L_0^{WF} is WF section average phase inductance and L_g^{WF} is WF section phase inductance amplitude variations above average.

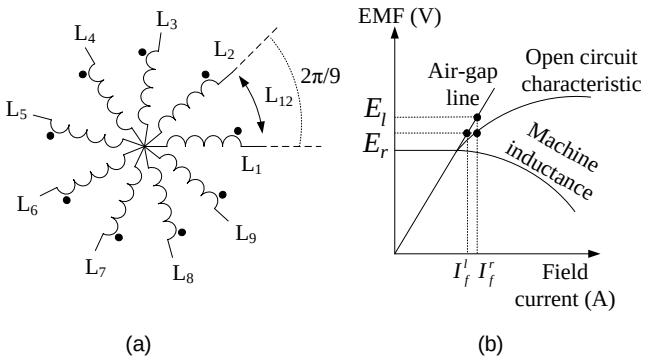

Fig. 8. HG inductance. (a) Coils arrangement. (b) Saturation effect.

Machine inductance is modified to account for the saturation effects discussed above via a saturation factor that is calculated using the machine open circuit characteristics [24]. Referring to Fig. 8(b) the saturation factor is defined as:

$$k_s = \frac{I_f^r}{I_f^l} = \frac{E_l}{E_r} \tag{2}$$

where, I_f^r is field current at rated stator load current, I_f^l is field current that produces rated back-EMF on the linear air-gap characteristic, E_l is back-EMF produced by rated rotor field current on the air-gap linear characteristic and E_r is rated back-EMF. The saturated inductance is obtained by dividing the unsaturated inductance by the saturation factor. Table II summarizes the HG main specifications.

C. HG Loss Audit

The losses in the HG are split into stator and rotor copper loss, stator iron loss and mechanical losses such as windage and friction. The iron losses are predicted via polynomial regression which is used to fit the curve of actual iron loss data of the machine laminations at different frequencies. The iron losses for 3 sections namely stator tooth tip, stator tooth

TABLE II
HG SPECIFICATION DETAILS

Parameter	WF section	PM section	HG
Output power (MW)	1.25	3.75	5
RMS phase voltage (kV)	2.7	8.1	10.80
Active axial length (mm)	100	421	521
Total axial length (mm)	120*	421	541
Number of turns per stator coil (p.u.)	12	12	12
Stator coil cross-section (mm^2)	380.64	380.64	380.64
Phase resistance (Ω) at 75°C	0.175	0.525	0.70
Number of turns per rotor coil (p.u.)	51	-	51
Rotor coil cross-section (mm^2)	5712	-	5712
Rotor resistance (Ω) at 75°C	0.078	-	0.078
Magnetic loading (T)	0.998	0.842	-
Stator slot current density (A/ mm^2)	3.94	3.94	3.94
Rotor slot current density (A/ mm^2)	4.34	-	-

*Considering end-winding for the WF rotor

TABLE III
HG VOLUME, MASS AND LOSS AUDIT

Section	Volume (m^3)	Mass (kg)
Stator copper	0.13252	1187.82
Rotor copper	0.0216	193.54
Total copper	0.15412	1381.36
Total stator steel	0.64	4928.9
Total rotor steel	0.3989	3050.18
Total mass* (tonnes)	-	10.17
	Losses	
	(kW)	(%)
Stator copper	91.7	50.8
Rotor copper	18.44	10.2
Windage and friction	54.62	30.3
Iron	15.64	8.7
Total	180.4	100
Efficiency (%)	95.23	95.23

* Lamination density = 7650 kg/m^3; Copper density = 8960 kg/m^3; PM density = 7500 kg/m^3; Total mass excludes shaft, machine casing, end caps, cooling system and other support structure.

This article has been accepted for publication in a future issue of this journal, but has not been fully edited. Content may change prior to final publication. Citation information: DOI 10.1109/TIE.2017.2748054, IEEE Transactions on Industrial Electronics

body and stator back-iron are calculated separately since they operate at different flux-densities and they are summed to obtain the HG total loss. Table III shows the HG volume, mass and loss audit. The stator and rotor copper losses contribute to 50.8% and 10.2% of the total loss, the windage and friction contribute to 30.3% and the iron loss is 8.7% of the total machine losses. The HG efficiency at 5 MW output is 95.23%.

D. HG Connected to a Passive Rectifier

A MATLAB/Simulink model is developed to simulate and compare the performance of 3- and 9-phase HGs. The MATLAB machine model incorporates FEA results for the machine back-EMF due to the PM and WF rotor sections and flux-linkage and currents (for the inductance calculations) into look-up tables. The machine model is connected to an uncontrolled 3- or 9-phase full-bridge rectifier with a battery load modeled as a fixed impedance and ideal voltage source. Control of the machine output is performed via adjusting the wound field current. The no-load rectified DC-link voltages for the 3- and 9-phase designs are shown in Fig. 9(a). The simulated average DC-link voltage is consistent with the analytical value i.e. 27.32 kV, giving confidence in the model accuracy. Table IV compares simulated 3- and 9-phase systems. The 9-phase design results in 4.2% higher RMS voltage and 20% higher DC-link rectified voltage and is, therefore, a justified option for the machine. Compared to the 3-phase design, the DC-link current in the 9-phase system is increased by 6% due to the contribution of higher phase voltage, including the improved winding factor, while the phase RMS current is reduced by 61%. The DC-link voltage ripple frequency in the 9-phase system is 3 times higher than the 3-phase system, which combined with the reduced magnitude, reduces the DC-link filter capacitance requirements.

TABLE IV
COMPARISON OF 3-PHASE AND 9-PHASE MACHINES AT RATED POWER

Items	3-phase	9-phase	Ratio 9φ/3φ
Rated power (MW)	5	5.2	1.04
No-load peak phase voltage (kV)	13.77	13.94	1.012
No-load RMS phase voltage (kV)	10.37	10.80	1.041
No-load average DC-link voltage (kV)	22.77	27.32	1.2
No-load peak DC-link voltage (kV)	23.85	27.45	1.151
No-load min. DC-link voltage (kV)	20.65	26.74	1.295
No-load peak to peak ripples (kV)	3.2 (13.4%)	0.71 (2.6%)	0.22
Average DC current (kA)	0.67	0.71	1.06
RMS phase current (kA)	0.69	0.27	0.39

IV. PROTOTYPE HG AND EXPERIMENTAL TEST FACILITY

The scope of this paper does not permit the build and test of a full power (5 MW) HG comparable with one suitable for the off-shore wind generation system in Fig. 2. However, to investigate the feasibility of the proposed HG concept a low power (3 kW) and low voltage (maximum peak phase voltage of 88.5 V at a rated speed of 3000 RPM) prototype HG is designed and test validated in the laboratory.

The prototype HG is analyzed and results compared against the test data to validate the analysis models and procedures. Having established the validity of the design procedure, these tools are then used to design the full power HG. The objectives are to develop a simulation model for the HG, use the model to investigate the machine operational characteristics when acting as a generator into a variable DC-link supply, validate the model experimentally and then propose the operational philosophy with-regard-to field control and DC-link interaction. The prototype HG is designed with a 25% WF to 75% PM split-ratio and as a 9-phase generator with 32 poles. The stator lamination has 36 slots with concentric coils. The PM rotor has 32 sintered NdFeB magnets and the WF rotor uses 32-slot laminations each wound with simple concentrated coils to form a 32-pole configuration as per the PM rotor section. Note that the PM and WF rotor share the same stator. For the prototype HG, the DC current for the WF is supplied via slip-rings and brushes. However, a brushless exciter utilizing the same stator and

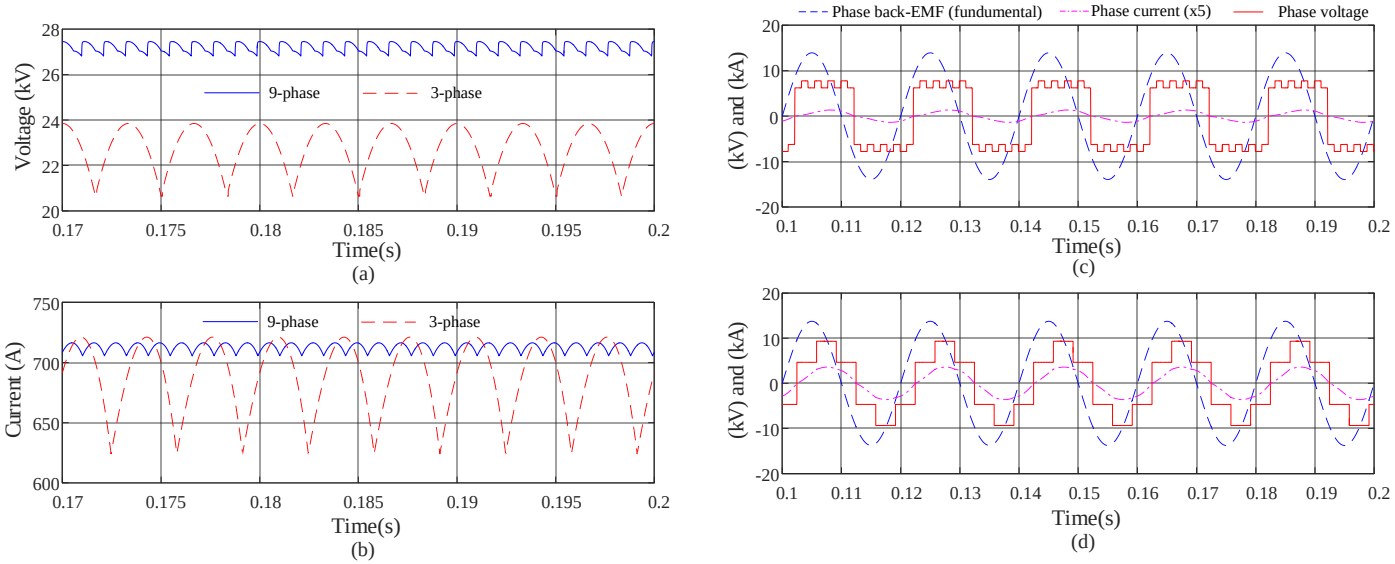

Fig. 9. HG performance characteristics 3- and 9-phase comparison. (a) Rectified DC-link voltage. (b) Rectified DC link current. (c) 9-phase voltage, current and EMF. (d) 3-phase voltage, current and EMF.

This article has been accepted for publication in a future issue of this journal, but has not been fully edited. Content may change prior to final publication. Citation information: DOI 10.1109/TIE.2017.2748054, IEEE Transactions on Industrial Electronics

rotor WF laminations has been designed by the authors as discussed in [19]. Table V lists the HG prototype and brushless exciter specifications while Fig. 10 shows prototype HG details. The HG 9-phase output is full-bridge rectified and connected to a controlled DC source that emulates the system DC-link. The HG assembly is housed in a single casing. The test-rig comprises of the laboratory prototype HG, in-line torque measurement transducer and a 4 kW electronically controlled industrial induction machine. The induction machine acts as a variable speed prime-mover emulating the wind turbine mechanical input to the HG.

The first test on the prototype machine is performed by measuring the open circuit back-EMF at nominal speed of 3000 rpm as shown in Fig. 11(a). The measured and predicted waveforms show a good correlation. In addition, the measured rectified open-circuit DC-link voltage at different speeds is plotted in Fig. 11(b). Results of a thermal test applied on the HG prototype machine to investigate the temperature rise in the stator tooth are presented in Fig. 11(c) for two different speeds. Compared to 1500 rpm a higher temperature rise is seen at 3000 rpm due to higher core losses. Fig. 11(d) shows the HG prototype simulation results for different delivered electrical power between 0.5 and 3 kW at 3000 RPM and for varying DC-link voltage. For each delivered power the WF current is chosen to match the HG rectified voltage to that of the test DC-link voltage. The characteristic is a set of V-curves, although these V-curves are not to be confused with classical V-curves for conventional wound rotor synchronous machines. Fig. 11(e) presents measured results at a nominal speed of 3000 RPM when delivering a fixed power of 2 kW and 3 kW to the DC-link. Compared to the 2 kW results, the curves for the 3 kW delivered power in Fig. 11(e) are shifted upwards due to higher WF current requirements. As seen from Fig. 11(e) the HG was tested to confirm the generator operational characteristics within a laboratory environment for a large range of DC-link voltage variation (40-140V). However, in practice, this variation exceeds the wind turbine application requirements (i.e. ±25% voltage variations), but is tested here to illustrate the generator characteristic outside the required envelope. As discussed earlier for the wind farm application, the maximum DC-link voltage variation among the turbines at each speed due to the WF is only 25% which results in a practical limit to the WF current (0-2A) and DC-link voltage variations (90 to 110V), as illustrated in Fig. 11(e). Therefore, as the wind velocity and hence HG rotor speed varies, the resulting DC-link voltage variation can be modified by variation of the WF rotor current to maintain output voltage and generation.

To investigate the WF saturation limit, the prototype HG was tested for an extended range of WF excitation current at the rated speed (≈ 3000 rpm), as illustrated in Fig. 11(f). The results show that the voltage induced by the WF rotor and hence the total back-EMF saturation starts when the excitation current is between 2.75 and 3 A. The perturbation in the stator voltage due to the PM rotor seen from Fig. 11(f) is due to the small speed variations around 3000 rpm from the prime mover. Fig. 12 compares simulations and test results of phase back-EMF, voltage and current, DC-link voltage and current of the HG prototype when delivering 2 kW at a speed of 3000 RPM to the DC-link with a battery voltage of 136.4 V. The results show the good agreement between simulated and measured data hence confidence in model accuracy and the design. As shown in Fig. 12 there are intervals where the phase current is zero due to the line-to-line machine back-EMF falling below the battery voltage and turn-off of the corresponding diodes. Therefore, in the zero current intervals the drop voltage across the machine impedance is zero and the phase voltage follows the back-EMF. Note that for the 5MW HG design simulations, the phase current in Fig. 9 does not

TABLE V
HG PROTOTYPE AND BRUSHLESS EXCITER SPECIFICATION

Description	Value
PM rotor axial length (mm)	25
WF rotor axial length (mm)	10
Brushless exciter axial length (mm)	4
Number of turns per stator coil for the HG	14
Number of turns per stator coil for the brushless exciter	50
Number of turns per rotor coil for the WF	80
Number of turns per rotor coil for the brushless exciter	73
Number of HG and exciter stator slots	36
Number of WF and exciter rotor lamination slots	32
Number of HG stator phases	9
Number of exciter rotor phases	16
Number of HG poles	32
Number of brushless exciter poles	36

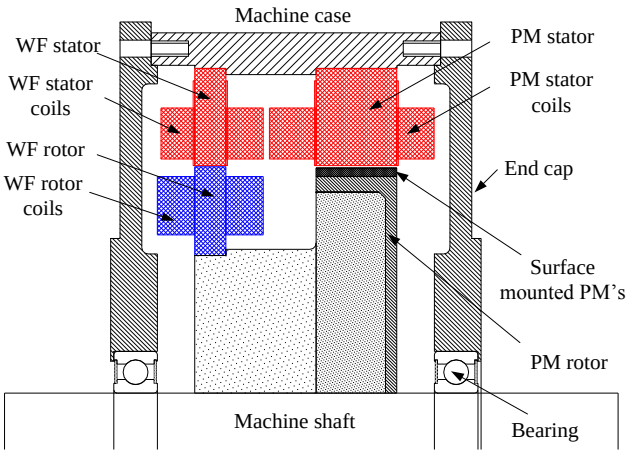

(a)

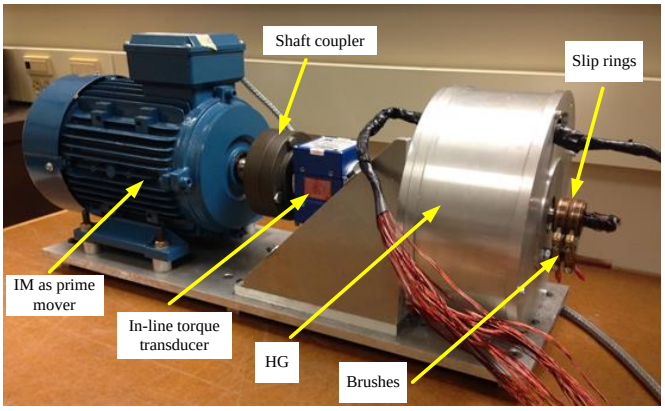

(b)

Fig. 10. HG Prototype. (a) Machine general assembly. (b) Test-rig.

fall to zero. Moreover, the difference in the perturbations in the peak phase voltage in the laboratory prototype, Fig. 12, and the 5MW design, Fig. 9, arises due to the difference in per-unit impedance between the two machines. The EMF to impedance ratio for the 5MW machine is around 9 times that of the laboratory prototype machine.

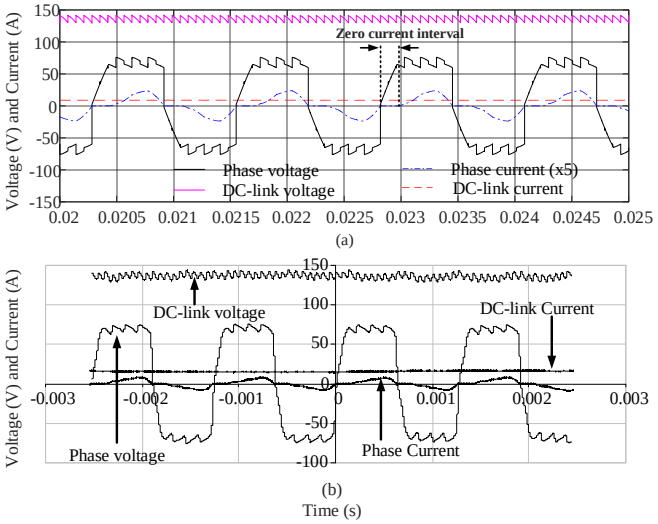

Fig. 12. HG phase voltage and current, DC-link voltage and current at 3000 RPM for a delivered power of 2 kW and for an average DC-link voltage of 136.4 V. (a) Simulation results. (b) Test results.

V. Conclusion

This paper proposes a high voltage hybrid generator (HG) conversion system for wind turbine applications. The proposed HG has two rotor sections, a wound field (WF) and a permanent magnet (PM) rotor. The two rotors share a 9-phase stator. Compared to a 3-phase design, the 9-phase HG yields improved power density while eliminating the smoothing DC-link capacitors that would otherwise be required. The choice of WF to PM split ratio is discussed based on the turbine operational characteristics and depending on the maximum wind velocity variations expected among turbines in a typical wind farm. Magnetically, the WF section operates lightly saturated at full-load, while the PM section operates in the linear region to limit magnet material. This facilitates a reduced HG inductance hence improving output power capability. The machine copper losses are calculated at the rated stator and rotor current while the iron loss is calculated for tooth tip, tooth body and back-iron separately since they operate at different flux-densities. The iron losses are predicted via polynomial regression that is used to fit the loss curves provided by lamination manufacturer. The measured results are in good agreement with the simulation results giving confidence in the accuracy and feasibility of the proposed system.

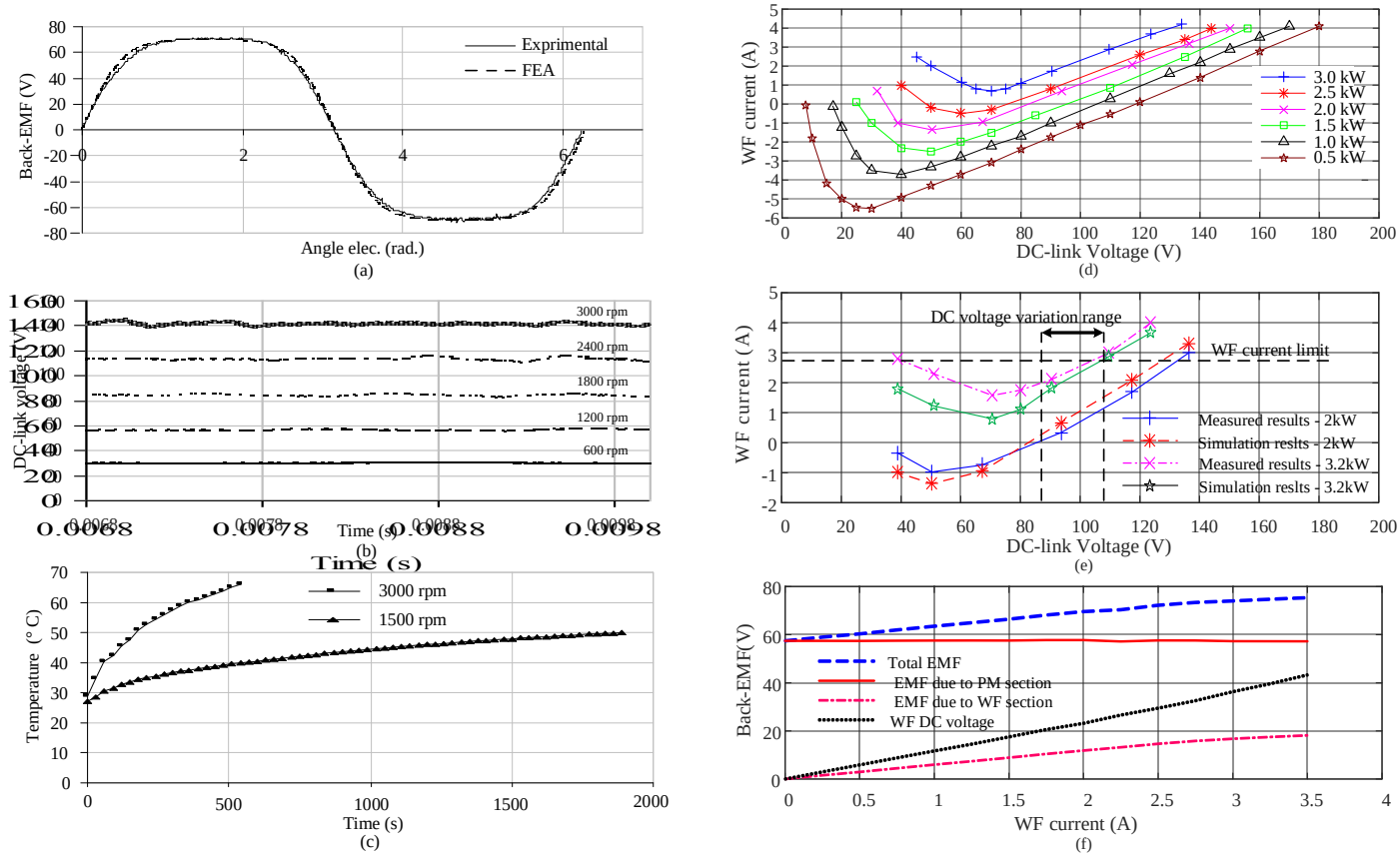

Fig. 11. HG prototype characteristics at 3000 RPM. (a) Predicted and measured back-EMF at 3000 rpm. (b) Measured open-circuit DC-link voltage at various speed. (c) Stator tooth temperature rise at full-load for 1500 rpm and 3000 rpm. (d) Simulation results for different load with varying DC-link voltage at 3000 rpm. (e) Test results for 2kW and 3.2kW delivered power with varying DC-link voltage at 3000 rpm. (f) Measured characteristics with extended range of the WF excitation current at 3000 rpm.

REFERENCES

[1] S. Muller, M. Deicke, R. W. De Doncker, "Doubly fed induction generator systems for wind turbines," *IEEE Industry Applications Magazine*, vol. 8, no. 3, pp. 26-33, May/Jun 2002.

[2] A. Gaillard, P. Poure, S. Saadate, M. Machmoumc, "Variable speed DFIG wind energy system for power generation and harmonic current mitigation," *Renewable Energy*, vol.34, pp.1545–1553, 2009.

[3] R. Pillai, S. Narayanan, G. Swindale, "Benefits and challenges of a grid coupled wound rotor synchronous generator in a wind turbine application," *Technical Report, Cummins Generator Technologies*, Issue number: WP102, 2016.

[4] J. A. Baroudi, V. Dinavahi. A.M. Knight, "A review of power converter topologies for wind generators", *Renewable Energy*, vol.32, pp.2369-2385, 2007.

[5] R. Datta, V.T. Ranganathan, "Variable-speed wind power generation using doubly fed wound rotor induction machine-a comparison with alternative schemes," *IEEE Transactions on Energy Conversion*, vol.17, no.3, pp.414-421, Sep. 2002.

[6] K.T. Chau, Y.B. Li, J.Z. Jiang, S. Niu, "Design and Control of a PM Brushless Hybrid Generator for Wind Power Application," *IEEE Transaction on Magnetics*, vol.42, no.10, pp.3497-3499, 2006.

[7] C. Liu, K.T. Chau, J.Z. Jiang, L. Jian, "Design of a New Outer-Rotor Permanent Magnet Hybrid Machine for Wind Power Generation," *IEEE Transaction on Magnetics*, vol.44, no.6, pp.1494-1497, 2008.

[8] H. Li, Z. Chen, "Overview of different wind generator systems and their comparisons," *IET Renewable Power Generation*, vol.2, no.2, pp.123-138, June 2008.

[9] D. J. Bang, H. Polinder, G. Shrestha, and J. A. Ferreira, "Review of generator systems for direct-drive wind turbines," *European Wind Energy Conference and Exhibition*, Belgium, Mar. 31–Apr. 3, 2008.

[10] H. Polinder, F. van der Pijl, G. de Vilder, P.J. Tavner, "Comparison of direct-drive and geared generator concepts for wind turbines," *IEEE Transaction on Energy Conversion*, vol.21, no.3, pp.725-733, 2006.

[11] M. Liserre, R. Cardenas, M. Molinas, J. Rodriguez, "Overview of Multi-MW Wind Turbines and Wind Parks," *IEEE Transactions on Industrial Electronics*, vol.58, no.4, pp.1081-1095, April 2011.

[12] DeWind D8.2 2000 kW wind turbine (2016). [Online]. Available: http://www.dewindco.com. Last accessed on April 2017.

[13] Avera M5000-116 power curve (2017). [Online]. Available: http://www.renugen.co.uk/content/large_wind_turbine_brochures/large_wind_turbine_brochures/areva_m5000.pdf. Last accessed on April 2017.

[14] O. Beik, N. Schofield, "Hybrid Generator for Wind Generation Systems", *IEEE Energy Conversion Congress and Exposition (ECCE 2014)*, Pittsburgh, PA, USA, Sept 14-18, 2014.

[15] European Wind Energy Association (EWEA), "The European offshore wind industry - key trends and statistics 1st half 2014" July 2014.

[16] O. Beik, N. Schofield, "An Off-Shore Wind Generation Scheme with High Voltage Hybrid Generator, HVDC Interconnections and Transmission" *IEEE Transactions on Power Delivery*, vol. 31, no. 2, pp. 867-877, April 2016.

[17] J. F. Gieras, *Advancements in Electric Machines*. Springer, Netherlands, 2010.

[18] S.J. Sugimoto, "Current status and recent topics of rare-earth permanent magnets," *Journal of Physics D: Applied Physics*, Volume 44, Issue 6, 2011.

[19] O. Beik, N. Schofield, "A Brushless Exciter Design for a Hybrid Permanent Magnet Generator Applied to Series Hybrid Electric Vehicles", *The 7th IET international conference on Power Electronics, Machines and Drives (PEMD 2014)*, Manchester, UK, April 8-10, pp. 1-6, 2014.

[20] D. Jovcic, N. Strachan, "Offshore wind farm with centralised power conversion and DC interconnection," *IET Generation, Transmission & Distribution*, vol.3, no.6, pp.586-595, 2009.

[21] J.L. Rodriguez-Amenedo, S. Arnalte, J.C. Burgos, "Automatic generation control of a wind farm with variable speed wind turbines," *IEEE Transactions on Energy Conversion*, vol.17, no.2, pp.279,284, Jun 2002.

[22] T. Surinkaew, I. Ngamroo, "Coordinated Robust Control of DFIG Wind Turbine and PSS for Stabilization of Power Oscillations Considering System Uncertainties," *IEEE Transactions on Sustainable Energy*, vol.5, no.3, pp.823-833, July 2014.

[23] M. Chinchilla, S. Arnaltes, J.C. Burgos, "Control of permanent-magnet generators applied to variable-speed wind-energy systems connected to the grid," *IEEE Transactions on Energy Conversion*, vol.21, no.1, pp.130-135, March 2006.

[24] V. Del Toro, *Electric Machines and Power Systems*. Prentice-Hall, N. J., 1985.

Omid Beik (S'14-M'16) received the B.Sc. degree (Hons.) with highest distinction in electrical engineering from Yazd University, Yazd, Iran (2007), the M.Sc. degree with highest distinction in electrical engineering from Shahid Beheshti University, Abbaspour School of Engineering, Tehran, Iran (2009) and the Ph.D. degree in electrical engineering from McMaster University, Hamilton, Ontario, Canada (2016). He was a Postgraduate Researcher with the Power Conversion Group at The University of Manchester, UK (2011-12) and a Postdoctoral Research Fellow McMaster Automotive Resource Center (MARC), Hamilton, Ontario, Canada (2016-17). He is currently a Senior Engineer with Magna Powertrain Inc., Toronto, Ontario, Canada. His main research is focused on electric machine design, drives and power electronics for applications in renewable energy systems and electrified powertrains.

Nigel Schofield (M'06) received the degrees of B.Eng. (Hons.) and Ph.D. from the University of Sheffield, UK, in 1990 and 1997, respectively. Dr. Schofield was at the University of Sheffield (1993-95; 1997-2004) and a Design Engineer in industry (1995-97). He was a Lecturer (2004-09) and Senior Lecturer (2009-12) in the School of Electrical and Electronic Engineering, at the University of Manchester, UK. He was Full Professor with Tenure in the Department of Electrical and Computer Engineering, McMaster University, Ontario, Canada (2013-17). In May 2017 he joined the University of Huddersfield, UK, as Professor of Electrical Engineering. Prof. Schofield is a member of the Institution of Engineering and Technology, U.K., and he is a Chartered Engineer in the U.K.